RSC Advances

ROYAL SOCIETY OF CHEMISTRY

www.rsc.org/advances

Cite this: DOI: 10.1039/c0xx00000x

www.rsc.org/xxxxxx

Communication

Electrochemical Role of Oxygen Containing Functional Groups on Activated Carbon Electrode

Tomohiro Tojo,[a] Kengo Sakurai,[b] Hiroyuki Muramatsu,[b] Takuya Hayashi,[b] Kap-Seung Yang,[c] Yong Chae Jung,[d] Cheol-Min Yang,[d] Morinobu Endo,[e] Yoong Ahm Kim[c,*]

Received (in XXX, XXX) Xth XXXXXXXXX 20XX, Accepted Xth XXXXXXXXX 20XX
DOI: 10.1039/b000000x

We have experimentally and theoretically clarified the effect of oxygen functional groups on capacitive performance of the photochemically treated activated carbon electrode. A high density of C=O group at the mouth of the micropores, where the chemically active edge sites are predominantly available, increase the energy barrier for ions to enter the pores, thereby resulting in a large decrease in the specific capacitance.

1. Introduction

Electric double layer capacitors (EDLC) have drawn much attention as one of the promising power sources for portable devices and electric vehicles because of their higher power density, better reversibility for charge-discharge, and longer cycling time than those of the lithium ion batteries. Such characteristics are based on their intrinsic operation mechanism, e.g. physical ion adsorption on a high surface area.[1] However, one of the major disadvantages of EDLC is their low energy density, because the amount of energy is proportional to the thickness of the electric double layer formed at the interface of any electrode and electrolyte.[1, 2] This charge-discharge capacitance can be classified into two groups– one is related to non-Faradaic reactions, where the capacitance is proportional to the amount of the stored ions between the electrodes; the other is related to capacitance, called as pseudo-capacitance, which is based on fast and reversible Faradaic reactions.[1, 2] Thus, to improve the energy density of EDLC, both physically occurring non-Faradaic reactions utilizing high surface area and chemically reversible Faradaic reactions need to be considered.

Various carbon materials, such as activated carbons, carbon nanotubes and graphene have been examined as electrode materials to achieve high capacitive performance of EDLC, because they exhibit high specific surface area, excellent mechanical strength, high electronic mobility and high chemical stability.[3] In particular, the functional groups on the surface of the carbon materials are crucial to improve the pseudo-capacitance. For example, foreign atoms, e.g. nitrogen, boron and oxygen are known to change the electrochemical behaviors, resulting in a decrease in the charge-transfer resistance on the surface.[4] In addition, the negatively charged oxygen functional groups were thought to improve the wettability of carbon based electrodes with respect to the electrolyte during Faradaic reactions.[5] Therefore, in order to enhance both electrostatic and pseudo capacitors' performance, it is required to analyze the effect of oxygen-containing functionalities and the pore size on the surface of the carbon materials.

Various carbon materials, containing oxygen functional groups have been synthesized via heat treatment of nitrogen and oxygen containing precursors,[4, 6] plasma treatment under an oxidative gas,[7] and chemical modification in acid solutions[8], in order to improve the pseudocapacitance of EDLC. It is reported that the highly reversible pseudocapacitance is mainly attributed to reversible active reactions of the electrochemically active oxygen functional groups between the hydroxyl and carbonyl groups.[9] Some theoretical and experimental studies have shown that the electronic characteristics at the active sites of the carbon materials for electrophilic or nucleophilic interactions, are changed as a result of large polarization on the edges or basal planes of modified carbon structures.[10] Thus, aqueous ions were thought to enter into the pores due to coulomb force, since the edge sites are chemically more active than the basal planes and thus, oxygen containing functional groups are more abundant at the mouth of the pores.[10]

It is generally accepted that the porosity and the pore size distribution are important factors to determine the total capacitance of carbon materials. Some authors suggested that the micropores below 2 nm are closely related with the total capacitance because of its high ion accessibility.[11]

Even though activated carbons with a controlled pore size, high specific surface area and low cost showed high capacitive performance in aqueous electrolyte,[12] no systematic study on the relation between the pore size and oxygen containing functional groups (e.g., epoxide, hydroxyl and carboxyl groups) has been reported to date. In the current work, variations in the capacitive performance of photochemically-treated activated carbon have been studied and the experimental results were further supported through theoretical calculation. The reason for choosing vacuum ultraviolet as a mild surface modification tool[13] is to introduce oxygen functional groups in a controllable fashion through minimal structural change of the activated carbon.

2. Experimental and theoretical details

2.1 Synthesis of activated carbon

Activated carbon was prepared as follows. The carbonized phenolic resin (Showa Denko K. K.) at 600 °C was chemically activated with potassium hydroxide at 800 °C for 1 h in argon. Potassium hydroxide was selected as the activating reagent to generate a high specific surface area and micropores. To introduce oxygen containing functional groups on the surface of the activated carbon, vacuum ultraviolet light (172 nm, Xe excimer lamp, Ushio UER20-172V) was irradiated on the activated carbons for 10, 30 and 60 min using the apparatus filled with O_2 gas (see Fig. S1).

2.2 Structural Characterizations

The macro-morphology of the active carbon before and after the vacuum ultraviolet irradiation was characterized by field emission scanning electron microscopy (JEOL JSM-6335F, 10 kV, Japan). X-ray powder diffraction patterns (Rigaku RINT-2200V PC, CuK_α (λ = 1.54056 Å)) were obtained to evaluate the crystallinity of the sample, and Raman spectra were recorded (Kaiser HoloLab 5000 system) using a 532 nm laser line. Surface elemental analysis was carried out with X-ray photoelectron spectroscopy (XPS, Axis-Ultra, Shimadzu Kratos Analytical) using a monochromator from Al target with an emission current of 15 mA and an accelerating voltage of 15 kV. The pore structure was characterized using nitrogen adsorption isotherm (Shimadzu ASAP 2020, Japan) at liquid nitrogen temperature.

2.3 Capacitor Performance and Electrochemical Analysis

The $2H^+$ and SO_4^{2-} storage behaviors of the pristine and the photochemically treated samples were evaluated by cyclic voltammetry (CV) using a standard three-electrode system (a platinum foil electrode as current collectors and an Ag/AgCl as a reference electrode). To prepare the working or the counter electrode, activated carbon (95 wt. %) was first mixed with poly(tetrafluoro ethylene) (5 wt. %) without any solvent. The activated carbon and binder were mixed using an agate mortar for 30 minutes in order to prepare homogeneous paste. The mixture was then pressed to form a disk-shaped electrode at a pressure of 9806 kPa. The disk was further mounted on a platinum current collector. The electrolyte, consisting of 1 M H_2SO_4 was bubbled with argon gas for more than 1 h to remove any dissolved oxygen under argon before the CV measurement. The total specific capacitance of each working electrode was measured with a potentiostat/galvanostat (an advanced electrochemical system model PARSTAT 2273 from Princeton Applied Research) at a scanning rate of 10 mV/s within a potential range of -0.2–0.8 V vs. Ag/AgCl.

2.4 Simulation Model and Conditions

We generated several models containing pores at the center of ABAB stacking graphite in which a series of oxygen functional groups were bonded at the edges of the pores (Fig. 1). The pore sizes were in the range from 12 Å × 12 Å to 25 Å × 25 Å and carbon atoms at the edge (or the mouth) of the pores were terminated by hydrogen (H) and oxygen functional groups (*e.g.*, C-OH, C=O, O-C=O and COOH). These models were built using the software *HyperChem. Professional* v. 7.0.1 (Hypercube, Inc.), which is commonly used for computational chemistry and as molecular modelling tools.[14] Structural optimization was performed with the classical force field.[15] The interlayer distance in the models, where the edges are open-ended and H-terminated was found to be 3.44 Å. On the other hand, the distance between the layers containing oxygen functional group was increased up to 5.7 Å.

These models were considered as initial structures for classical molecular dynamics (MD) simulation to reveal the behavior of the ions within the graphite pore and the energy barrier. The MD simulation was done by *Xenoview* software[16] for 30 ps with 0.1 fs time steps and 298 K under periodic boundary condition in all direction, using a consistent valence force field potential,[17] which was useful to understand the interaction between atoms or molecules, such as organic materials and solvents. The energy barrier was calculated from the penetrating energy of hydrated SO_4^{2-} ion into each pore.

Using the *Car-Parrinello Molecular Dynamics* code[18] v. 3.11.1, the binding (adsorption) energy of the SO_4^{2-} ions to the edges was calculated, using the structures obtained from classical MD. The binding energies (E_B) were calculated by the following formula–

$$E_B = E_{\text{Graphite + ion}} - (E_{\text{Graphite}} + E_{\text{ion}}), \quad (1)$$

where $E_{\text{Graphite + ion}}$, E_{Graphite} and E_{ion} denote total energy of graphite with adsorbed SO_4^{2-}, the isolated graphite and an SO_4^{2-} ion, respectively. The norm-conserving Troullier-Martins pseudo-potentials[19] were chosen to express all the core electrons. To describe hydrogen bonding in water and at the vicinity of the modified carbon edges, we employed a generalized gradient approximation using the exchange-correlation potential of Becke-Lee-Yang-Parr.[20] A total energy convergence of 1 × 10^{-7} Hartree and the plane wave cut-off energy of 70 Rydberg were adapted in order to obtain accurate calculations.

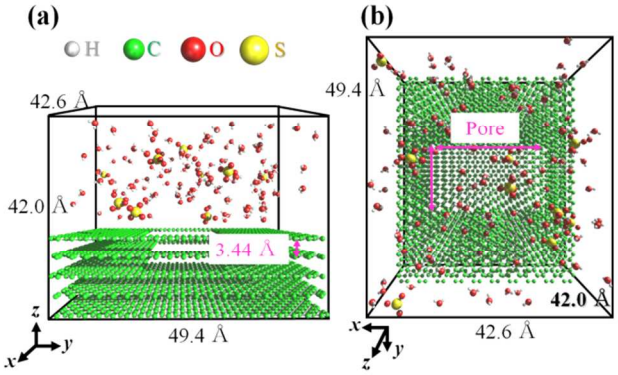

Fig. 1 Simulation model of (a) side view, and (b) top view.

3. Results and discussion

XPS measurements were performed in order to obtain the compositional change caused by vacuum ultraviolet irradiation. Figure 2 shows C 1*s* spectra of the pristine and the photochemically-treated activated carbons at various times. The C 1*s* spectrum displays five peaks[21] at 284.5, 285.0, 286.2, 286.9-287.8 and 288.4-289.5 eV, which can be assigned to sp^2-bonded carbon, sp^3-bonded carbon, phenolic/ethereal bond, carbonyl bond and carboxyl bond, respectively. The relative amount of

oxygen containing functional groups from the C 1*s* spectra (Fig. 2) has been summarized in Table 1. A progressive increase in the amount of C-O and C=O groups with increasing irradiation time was observed. The increase in the relative percentage of these groups as well as shifting of the peaks toward the higher binding energy, indicate that oxidative reactions on the surface of the activated carbon occurred progressively.

To evaluate the structural defects on the surface of activated carbon caused by ultraviolet irradiation, Raman spectra were run using a 532 excitation laser line (Fig. 3 (a)). There were two main peaks[22], namely, the D-band (A_{1g} defect-induced mode) around 1325 cm^{-1} and the G-band (E_{2g2} graphite mode) at 1600 cm^{-1}, respectively.[23] The frequencies of both these bands remained unchanged before and after the ultraviolet irradiation, however, a decrease in the *R* value (the integrated intensity of the D band divided by the integrated intensity of the G band)[22] with increasing irradiation time was observed. In addition, we observed a substantial decrease of an amorphous sp^2 carbon bonded phase from the progressive decrease in the intensity of the D"-band around 1500 cm^{-1},[24] and also a decrease in the sp^2- and sp^3-bonded carbon contents in Table 1. The unusual decrease in the *R* value with increasing irradiation time suggested that the structural perturbation in the in-plane aromatic lattices can be repaired partially by introducing the large amount of C-O and C=O groups substitutionally or at the edges,[25] even though there was no change in their macro-morphology (Fig. S2). X-ray diffraction patterns were recorded to see the change in the crystallinity of the activated carbon before and after the ultraviolet irradiation (Fig. 3 (b)). All samples have broad *(002)* reflections at 2θ = 26°, indicative of disordered stacking structures, such as surface-modified carbons or amorphous carbons.[26] However, the intensities of the *(100)* and the *(102)* reflections at 2θ = 43° and 50°, respectively became weak with increasing irradiation time. The disappearance of *(100)* reflections indicated a structural change in the in-plane lattice on introduction of oxygen containing functional groups into graphite.

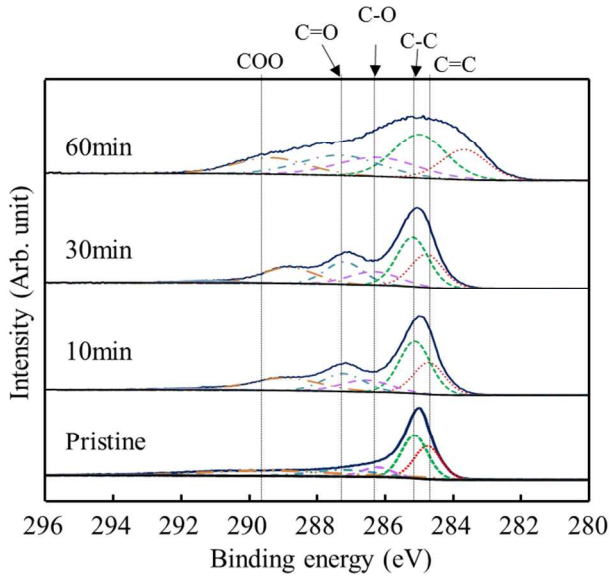

Fig. 2 The C 1*s* XPS spectra of the pristine and the ultraviolet irradiated activated carbons for 10, 30 and 60 min. Note that all spectra are curve-fitted to five peaks at 284.5, 285.0, 286.2, 286.9-287.8 and 288.4-289.5 eV, corresponding to sp^2- bonded carbon, sp^3-bonded carbon, C-O single bond, C=O double bond and O-C=O bond, respectively.

Table 1 The change in the relative concentration of oxygen-containing functional groups for the pristine and the ultraviolet irradiated activated carbons.

Bond type	*Pristine*	*Irradiation time* (min)		
		10	30	60
C=C (%)	25.94	21.88	21.02	17.30
C-C (%)	33.07	31.44	30.86	29.25
C-O (%)	8.885	11.63	12.85	18.88
C=O (%)	11.81	14.94	16.58	20.06
O-C=O (%)	19.20	18.14	16.65	14.51

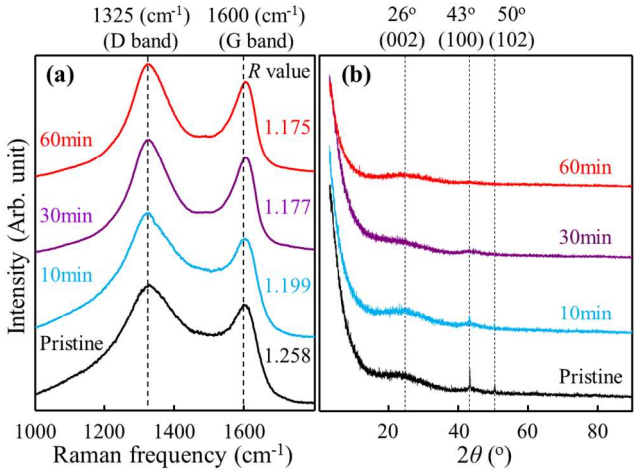

Fig. 3 (a) Raman spectra using a 532 nm laser line, and (b) X-ray diffraction patterns of the pristine and the ultraviolet irradiated activated carbons for 10, 30 and 60 min under O_2 gas.

In order to understand the effect of oxygen functional groups on electrochemical behaviours, we measured cyclic voltammetry (CV) of activated carbon before and after ultraviolet irradiation (Fig. 4 (a)). The pristine exhibited a relatively rectangular CV, as well as some small peaks around 0.45 V in forward scan and 0.3 V in reverse scan.[27] By contrast, for ultraviolet irradiated samples, CVs were largely distorted and the redox peaks disappeared. It has already been reported that the distortion of CVs at a high scan rate can be explained by the inaccessibility of aqueous ions to the micropores.[28] Moreover, we observed a substantial change in both the pore volume and pore size distribution from mesopores (2-50 nm in diameter) to micropores (~2 nm) via ultraviolet irradiation (Fig. 4 (b)).

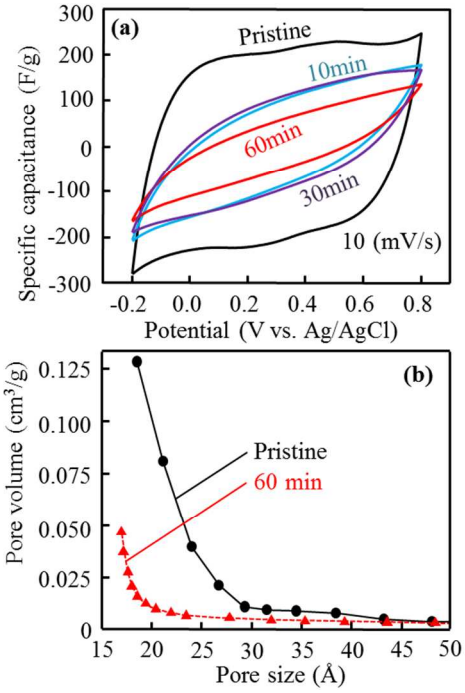

Fig. 4 (a) CV curves at a scan rate of 10 mV/s, and (b) pore size distribution of activated carbons before and after ultraviolet irradiation. Note that the mesopore size was calculated using Barret-Joyner-Halenda method.

Finally, in order to support the unusual capacitive behaviors of the ultraviolet irradiated activated carbons, the energy barrier for different sized pores, containing several types of oxygen functional groups was calculated using classical molecular dynamics simulation. Figure 5 shows a decrease in the energy barriers of the pores when the edges are H-terminated, open-ended, C-OH-, COO- and COOH-terminated edges in order. Such results indicate that the adsorption/desorption of ions can be promoted by introducing oxygen functional groups at the entrance of the pores. However, the energy barrier in the pore containing C=O was two times higher than those of other groups. The energy barrier of the pores containing C=O increased with decreasing pore size. In addition, the localized energy barrier near edges was in the range of 0.8-1.8 eV in pores where the edges were open-ended and terminated with hydrogen, C-OH, COO and COOH. However, we observed that, the maximized energy barrier (ca. 4.8 eV) was in the pores containing C=O. Here, the pores where the edges are terminated with COOH and C=O were mainly focused, because molecular orbitals in the C=O- and COOH-terminated edges are σ-bond-type and π-bond-type, respectively. By penetrating an SO_4^{2-} ion into the C=O- and COOH-terminated edges, the binding energy was calculated, using Car-Pirandello molecular dynamics with electronic structure simulations. The SO_4^{2-} ions at various sites were found to have higher binding energy (E_B = 1.87 eV) for C=O-terminated edge than that (E_B = 0.20 eV) for COOH-terminated edge. Thus it is expected that the unpaired electron of C=O plays an important role in the strong adsorption and/or repulsion of ions and the weak intermolecular force of COOH contributes to the easy desorption of ions. For comparison, hydrophobic carbon nanotubes[29] were irradiated with the vacuum ultraviolet for 60 min under same conditions. We observed a large amount of O-C=O (*i.e.*, COOH) and C=O (Table S1), and redox peaks in the CV of the vacuum ultraviolet irradiated carbon nanotube (Fig. S3). Such controversial result suggests that, the substantial decrease in capacitances of the vacuum ultraviolet irradiated activated carbon is due to the decrease in pore size, which limits the adsorption/desorption of ions, as well as the high density of C=O groups with high energy barrier and chemisorption energy at the entrances of the pores.

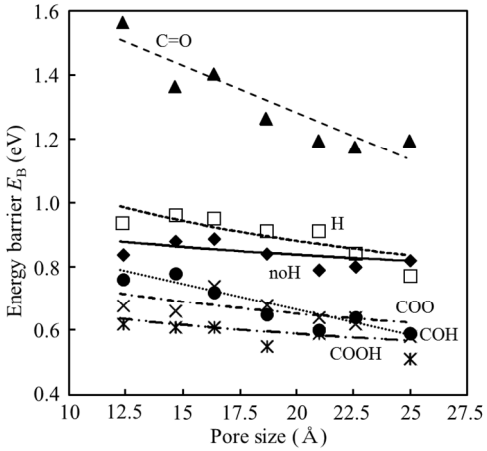

Fig. 5 The calculated energy barriers at the entrance of pores containing different types of oxygen functional groups.

4. Conclusions

We examined the effect of the vacuum ultraviolet irradiation on the electrochemical behaviors of activated carbons. We found an increase in the amount of CO group and decrease of sp^2/sp^3 carbons and O-C=O base with increasing irradiation time. Such change can be explained by CO groups' repairing ability for in-plane carbon lattice, as identified by the decrease of *R* value and the disappearance of *(100)* reflection by vacuum ultraviolet irradiation. Unexpectedly, the vacuum ultraviolet irradiation led to a substantial drop in the capacitance due to a large decrease in the pore size distribution. Using a molecular dynamic simulation study, it was revealed that the pores containing a large number of C=O group show the highest energy barrier (ca. 4.8 eV) with regard to SO_4^{2-} ions. In contrary, the COH, COO and COOH groups at the entrance of pores exhibited low energy barriers and thus promoted the adsorption/desorption of ions. From the viewpoint of carbon surface engineering, it is therefore, important to tailor the surface properties of porous carbons with oxygen functional groups.

Acknowledgements

Y.A.K acknowledges the financial support from Chonnam National University, 2013. Y.A.K and K.S.Y acknowledge the support from Global Research Laboratory (K2090300202412E010004010) through the National Research Foundation of Korea (NRF) funded by the Ministry of Science, ICT (Information and Communication Technologies) and Future Planning.

Notes and references

[a]*Department of Electrical and Electronic Information Engineering, Toyohashi University of Technology, 1-1 Hibarigaoka, Tempaku-cho, Toyohashi, Aichi 441-8580, Japan.*
[b]*Faculty of Engineering, Shinshu University, 4-17-1 Wakasato, Nagano 380-8553, Japan.*
[c]*School of Polymer Science and Engineering, Chonnam National University, 77 Yongbong-ro, Buk-gu, Gwangju 500-757, Republic of Korea. Fax: +82-62-530-1871; Tel: +82-62-530-1779; E-mail: yak@jnu.ac.kr*
[d]*Institute of Advanced Composite Materials, Korea Institute of Science and Technology (KIST), Eunhari san 101, Bongdong-eup, Wanju-gun, Jeonbuk 565-905, Republic of Korea.*
[e]*Carbon Institute of Science and Technology, Shinshu University, 4-17-1 Wakasato, Nagano 380-8553, Japan.*

† Electronic Supplementary Information (ESI) available: [Vacuum chamber with a vacuum ultraviolet light system (Fig. S1). SEM images of activated carbons before and after vacuum ultraviolet irradiation (Fig. S2). Atomic composition from C 1*s* spectra (Table S1) and cyclic voltamograms of carbon nanotubes before and after vacuum ultraviolet irradiation (Fig. S3).]. See DOI: 10.1039/b000000x/

1 E. Frackowiak and F. Béguin, *Carbon*, 2001, **39**, 937; A. Burke, *J. Power Sour.*, 2000, **91**, 37; M. Winter and R. J. Brodd, *Chem. Rev.*, 2004, **104**, 4245.
2 R. Kötz and M. Carlen, *Electrochim. Acta*, 2000, **45**, 2483; J. Chmiola, G. Yushin, Y. Gogotsi, C. Portet, P. Simon and P. L. Taberna, *Science*, 2006, **313**, 1760.
3 D. Qu and H. Shi, *J. Power Sour.*, 1998, **74**, 99; J. L. Figueiredo, M. F. R. Pereira, M. M. A. Freitas and J. J. M. Órfão, *Carbon*, 1999, **37**, 1379; M. S. Dresselhaus, G. Dresselhaus and P. C. Eklund, *Science of Fullerenes and Carbon Nanotubes*, Academic Press, New York, 1996; A. Jorio, M. S. Dresselhaus and G. Dresselhaus, *Carbon Nanotubes: Advanced Topics in the Synthesis, Structure, Properties and Applications*, Springer, New York, 2008; K. Balasubramanian and M. Burghard, *Small*, 2005, **1**, 180; H. Dai, *Acc. Chem. Res.*, 2002, **35**, 1035; K. S. Novoselov, A. K. Geim, S. V. Morozov, D. Jiang, Y. Zhang, S. V. Dubonos, I. V. Grigorieva and A. A. Firsov, *Science*, 2004, **306**, 666; A. K. Geim and K. S. Novoselov, *Nat. Mater.*, 2007, **6**, 183; M. J. Allen, V. C. Tung and R. B. Kaner, *Chem. Rev.*, 2010, **110**, 132.
4 Y. Qiu, X. Zhang and S. Yang, *Phys. Chem. Chem. Phys.*, 2011, **13**, 12554; L. Sun, L. Wang, C. Tian, T. Tan, Y. Xie, K. Shi, M. Li and H. Fu, *RSC adv.*, 2012, **2**, 4498; X. Y. Chen, C. Chen, Z. J. Zhang, D. H. Xie, X. Deng and J. W. Liu, *J. Power Sour.*, 2013, **230**, 50; K. Fujisawa, R. Cruz-Silva, K.-S. Yang, Y. A. Kim, T. Hayashi, M. Endo, M. Terrones and M. S. Dresselhaus, *J. Mater. Chem. A* 2014, **2**, 9532.
5 E. Raymundo-Piñero, F. Leroux and F. Béguin, *Adv. Mater.*, 2006, **18**, 1877; Y. Li, M. van Zijll, S. Chiang and N. Pan, *J. Power Sour.*, 2011, **196**, 6003; M. J. Bleda-Martínez, D. Lozano-Castelló, E. Morallón, D. Cazorla-Amorós and A. Linares-Solano, *Carbon*, 2006, **44**, 2642.
6 W. Li, D. Chen, Z. Li, Y. Shi, Y. Wan, G. Wang, Z. Jiang and D. Zhao, *Carbon*, 2007, **45**, 1757; C. O. Ania, V. Khomenko, E. Raymundo-Piñero, J. B. Parra and F. Béguin, *Adv. Funct. Mater.*, 2007, **17**, 1828.
7 A. Felten, C. Bittencourt, J. J. Pireaux, G. Van Lier and J. C. Charlier, *J. Appl. Phys.*, 2005, **98**, 074308; G. Zhang, S. Sun, D. Yang, J.-P. Dodelet, E. Sacher, *Carbon*, 2008, **46**, 196.
8 H. Oda, A. Yamashita, S. Minoura, M. Okamoto and T. Morimoto, *J. Power Sour.*, 2006, **158**, 1510; N. D. Kim, W. Kim, J. B. Joo, S. Oh, P. Kim, Y. Kim and J. Yi, *J. Power Sour.*, 2008, **180**, 671.
9 X. Fan, Y. Lu, H. Xu, X. Kong and J. Wang, *J. Mater. Chem.*, 2011, **21**, 18753; C.-Y. Yin, M. Aroua and W. Daud, *Sep. and Pur. Tech.*, 2007, **52**, 403.
10 D. C. Arriagada, *J. Mol. Model.*, 2013, **19**, 919; T. Schiros, D. Nordlund, L. Pálová, D. Prezzi, L. Zhao, K. S. Kim, U. Wurstbauer, C. Gutiérrez, D. Delongchamp, C. Jaye, D. Fischer, H. Ogasawara, L. G. M. Pettersson, D. R. Reichman, P. Kim, M. S. Hybertsen and A. N. Pasupathy, *Nano Lett.*, 2012, **12**, 4025; Y. J. Kim, C. M. Yang, K. C. Park, K. Kaneko, Y. A. Kim, M. Noguchi, T. Fujino, S. Oyama, M. Endo, *ChemSusChem*, 2012, **5**, 535.
11 P. Simon and Y. Gogotsi, *Acc. Chem. Res.*, 2013, **46**, 1094; G. Gryglewicz, J. Machnikowski, E. Lorenc-Grabowska, G. Lota and E. Frackowiak, *Electrochim. Acta*, 2005, **50**, 1197.
12 V. Ruiz, C. Blanco, M. Granda and R. Santamaría, *Electrochim. Acta*, 2008, **54**, 305.
13 S. H. Lee, Y. C. Jung, Y. A. Kim, H. Muramatsu, K. Teshima, S. Oishi and M. Endo, *Nanotechnology* 2009, **20**, 105708.
14 *Hyperchem.* Release 7 for Windows user manual, Molecular Modeling System, Hypercube, Inc., 2002.
15 B. R. Brooks, R. E. Bruccoleri, B. D. Olafson, D. J. States, S. Swaminathan and M. Karplus, *J. Comput. Chem.*, 1983, **4**, 187; A. D. MacKerell, Jr., D. Bashford, M. Bellott, R. L. Dunbrack, Jr., J. D. Evanseck, M. J. Field, S. Fischer, J. Gao, H. Guo, S. Ha, D. Joseph-McCarthy, L. Kuchnir, K. Kuczera, F. T. K. Lau, C. Mattos, S. Michnick, T. Ngo, D. T. Nguyen, B. Prodhom, W. E. Reiher, III, B. Roux, M. Schlenkrich, J. C. Smith, R. Stote, J. Straub, M. Watanabe, J. Wiórkiewicz-Kuczera, D. Yin and M. Karplus, *J. Phys. Chem. B*, 1998, **102**, 3586; K. Sint, B. Wang and P. Král, *J. Am. Chem. Soc.*, 2008, **130**, 16448.
16 S. Shenogin and Rahmi Ozisik, *Xenoview*: visualization for atomistic simulations, 2007; S. Shenogin, A. Bodapati, L. Xue, R. Ozisik and P. Keblinski, *Appl. Phys. Lett.*, 2004, **85**, 2229; S. Shenogin and Rahmi Ozisik, *J. Polym. Sci., Part B*, 2005, **43**, 994.
17 W. D. Cornell, P. Cieplak, C. I. Bayly, I. R. Gould, K. M. Merz, D. M. Ferguson, D. C. Spellmeyer, T. Fox, J. W. Caldwell and P. A. Kollman, *J. Am. Chem. Soc.*, 1995, **117**, 5179; J. R. Maple, Uri Dinur and A. T. Hagler, *Proc. Natl. Acad. Sci. USA*, 1998, **85**, 5350.
18 *Car-Parrinello Molecular Dynamics*, *CPMD* version 3.11.1, IBM Research Division and MPI Festkoerperforschung Stuttgart, 2007.
19 N. Troullier and J. L. Martins, *Solid State Commun.*, 1990, **74**, 613; N. Troullier and J. L. Martins, *Phys. Rev. B*, 1991, **43**, 1993.
20 A. D. Becke, *Phys. Rev. A*, 1988, **38**, 3098; C. Lee, W. Yang and R. G. Parr, *Phys. Rev. B*, 1988, **37**, 785.
21 A. M. Puziy, O. I. Poddubnaya, R. P. Socha, J. Gurgul and M. Wisniewski, *Carbon*, 2008, **46**, 2113; S. Park, K.-S. Lee, G. Bozoklu, W. Cai, S.-B. T. Nguyen and R. S. Ruoff, *ACS Nano*, 2008, **2**, 572; H. Murphy, P. Papakonstantinou and T. I. T. Okpalugo, *J. Vac. Sci. Technol. B*, 2006, **24**, 715.
22 M. S. Dresselhaus, G. Dresselhaus, R. Saito and A. Jorio, *Phys. Rep.*, 2005, **409**, 47; M. A. Pimenta, G. Dresselhaus, M. S. Dresselhaus, L. G. Cançado, A. Jorio and R. Saito, *Phys. Chem. Chem. Phys.*, 2007, **9**, 1276; M. S. Dresselhaus, A. Jorio, M. Hofmann, G. Dresselhaus and R. Saito, *Nano Lett.*, 2010, **10**, 751.
23 N. Kishore, S. Sachan, K. N. Rai and A. Kumar, *Carbon*, 2003, **41**, 2961; H.-K. Jeong, Y. P. Lee, R. J. W. E. Lahaye, M.-H. Park, K. H. An, I. J. Kim, C.-W. Yang, C. Y. Park, R. S. Ruoff and Y. H. Lee, *J. Am. Chem. Soc.*, 2008, **130**, 1362.
24 J. Schwan, S. Ulrich, V. Batori, H. Ehrhardt and S. R. P. Silva, *J. Appl. Phys.*, 1996, **80**, 440; R. E. Shroder, R. J. Nemanich and J. T. Glass, *Phys. Rev. B*, 1990, **41**, 3738.
25 P. Xue, J. Gao, Y. Bao, J. Wang, Q. Li and C. Wu, *Carbon*, 2011, **49**, 3346.
26 A. B. Bourlinos, D. Gournis, D. Petridis, T. Szabó, A. Szeri and I. Dékány, *Langmuir*, 2003, **19**, 6050; J. Zhao, L. Yang, F. Li, R. Yu and C. Jin, *Carbon*, 2009, **47**, 744; H. K. Jeong, M. H. Jin, K. P. So, S. C. Lim and Y. H. Lee, *J. Phys. D: Appl. Phys.*, 2009, **42**, 065418.
27 K. H. An, K. K. Jeon, J. K. Heo, S. C. Lim, D. J. Bae and Y. H. Lee, *J. Electrochem. Soc.*, 2002, **149**, A1058.
28 C.-H. Hou, C. Liang, S. Yiacoumi, S. Dai and C. Tsouris, *J. Colloid Interface Sci.*, 2006, **302**, 54; K.-L. Yang, S. Yiacoumi and C. Tsouris, *J. Electroanal. Chem.*, 2003, **540**, 159.
29 Y. Tao, H. Muramatsu, M. Endo, K. Kaneko, *J. Am. Chem. Soc.* 2010, **132**, 1214.

The table of contents entry

C=O groups at the mouth of micropores increase energy barrier for ions to enter the pores, resulting in a large decrease in the specific capacitance

Keywords (Activated carbon, Vacuum ultraviolet, Capacitor, Aqueous ion, Energy barrier)

T. Tojo, K. Sakurai, H. Muramatsu, T. Hayashi, K. S. Yang, Y. C. Jung, C-M. Yang, M. Endo, Y. A. Kim,*

Title: Electrochemical Role of Oxygen Containing Functional Groups on Activated Carbon Electrode